Published in final edited form as:
Biochim Biophys Acta. 2010 July ; 1803(7): 872–880. doi:10.1016/j.bbamcr.2010.04.007.

gp-91 mediates histone deacetylase inhibition-induced cardioprotection

Ting C Zhao[a,*], **Ling X Zhang**[b], **Guangmao Cheng**[c], and **Jun T Liu**[d]

[a]Department of Surgery, Roger William Medical Center, Boston University Medical School, Providence, RI 02908

[b]Department of Medicine, Rhode Island Hospital, Brown Medical School, Brown University, Providence, RI 02905

[c]Department of Medicine, Medical University of South Carolina, Charleston, SC 29403

[d]Department of Pharmacology, School of Medicine, Xian Jiao Tong University, Xian, Shanxi 710061, China

Abstract

We have recently shown that the inhibition of histone deacetylases (HDAC) protects the heart against ischemia and reperfusion (I/R) injury. The mechanism by which HDAC inhibition induces cardioprotection remains unknown. We sought to investigate whether the genetic disruption of gp-91, a subunit of NADPH-oxidase, would mitigate cardioprotection of HDAC inhibition. Wild-type and gp-91$^{-/-}$ mice were treated with a potent inhibitor of HDACs, trichostatin A (TSA, 0.1mg/kg, i.p.). Twenty-four hours later, the perfused hearts were subjected to 30 min of ischemia and 30 min of reperfusion. HDAC inhibition in wild-type mice produced marked improvements in ventricular functional recovery and the reduction of infarct size. TSA-induced cardioprotection was eliminated with genetic deletion of gp91. Notably, Western blot and immunostaining displayed a significant increase in gp-91 in myocardium following HDAC inhibition, which resulted in a mildly subsequent increase in the production of reactive oxygen species (ROS). The pretreatment of H9c2 cardiomyoblasts with TSA (50 nmol/L) decreased cell necrosis and increased viability in response to simulated ischemia (SI), which was abrogated by the transfection of cells with gp-91 siRNA, but not by scrambled siRNA. Furthermore, treatment of PLB-985 gp91$^{+/+}$cells with TSA increased the resistance to SI, which also diminished with genetic disruption of gp91 in gp91^{phox}-deficient PLB-985 cells. TSA treatment inhibited the increased active caspase-3 in H9c2 cardiomyoblasts and PLB-985 gp91$^{+/+}$cells exposed to SI, which were prevented by knockdown of gp-91 by siRNA. These results suggest that a cascade consisting of gp-91 and HDAC inhibition plays an essential role in orchestrating the cardioprotective effect.

Keywords

Histone deacetylase; gp-91; NADPH-oxidase; ischemia; myocardial infarction

*Corresponding Author: Fax: 401-456-4812; Tel: 401-456-8266. tzhao@rwmc.org.

1. Introduction

Histone acetyltransferases (HAT) and histone deacetylases (HDAC) have recently garnered the attention because they have emerged as an important mechanism in the regulation of a variety of cellular responses. Histone acetylation is mediated by histone acetyltransferase, which results in the modification of the structure of chromatin leading to nucleosomal relaxation and altered transcriptional activation. In contrast, the reverse reaction is mediated by histone deacetylase which induces deacetylation, chromatin condensation, and transcriptional repression (1–5). The acetylation status of the histone tails is determined by the interplay between HATs and HDACs. The opposing actions of HAT and HDACs allow gene expression to be exquisitely regulated through chromatin remodeling.

Since the identification of HDAC 1 (named HD 1) (6), over a dozen of HDACs have been described in mammals (7). These HDACs can be categorized into three distinct classes. Class I HDACs consist of HDAC 1, 2, 3, and 8, which are ubiquitously expressed and predominantly located in nuclei. Class II HDACs include HDAC 4, 5, 7 and 9. In contrast to class I, class II HDACs exhibit a tissue specific pattern of expression. HDAC 4 and HDAC 5 are found highly expressed in the heart, brain, and skeletal muscle and shuttle between the nucleus and cytoplasm (8–10). We have recently demonstrated that the inhibition of histone deacetylase with a selective inhibitor, trichostatin A, showed cardioprotective effects against I/R injury (12). This is consistent with the observations that the inhibition of HDAC in myocytes silences the fetal gene activation, blocks cardiac hypertrophy and prevents cardiac remodeling (13–15). Furthermore, HDAC inhibition has previously been shown to markedly decrease infarct size and reduce ischemia-induced neurological deficit scores in focal cerebral ischemia model of rats (16).

ROS have a central role in diverse physiological and pathological processes. When produced in large amounts by professional immune cells such as neutrophil granulocytes, ROS have antimicrobial activity serving in the first line of host defense (17). However, ROS produced at low levels by non-immune cell have been implicated in growth factor signaling, mitogenic response, apoptosis, and oxygen sensing (18–19). Our study has suggested that a mild generation of ROS protected the heart against myocardial necrosis (20). A plethora of evidence has well indicated that endothelial cells and vascular smooth muscle cells express an ROS generating, NADH/NADPH-dependent oxidase containing gp-91, a NADPH oxidase subunit, which is a membrane bound component of NADPH oxidase (21–23). In addition to these membrane-bound complexes, several other cytosolic proteins, including p67, p47, p40 and rac, translocate to the membrane and associate with the gp-91 subunits and p22 phox to assemble an enzyme complex that facilitate electron transfer from NADPH to molecular oxygen, leading to the generation of superoxides (24). Even though the investigations have supported that ROS generate a preconditioning effect to confer protection, the role of gp-91 attributable to this event remains unknown. Particularly, the inhibition of HDACs has been shown to result in the generation of ROS in tumor cell lines (25). The beneficial effects of mild ROS in preconditioned hearts were well addressed and HDAC inhibition has been shown to effectively trigger a generation of ROS. However, it also leaves the question open as to whether HDAC inhibition co-ordinates with gp-91 to transduce a signaling pathway to protect the heart against I/R injury. In this study, we investigated: 1) whether the cardioprotective effects induced with HDAC inhibitor, TSA, could be diminished with the targeted deletion of gp-91; 2) whether HDAC inhibition would enhance gp-91 of NADPH oxidase and ROS production in myocardium; 3) whether genetic suppression of gp-91 with siRNA would eliminate the resistance of H9c2 cardiomyoblast cells in response to simulated ischemia in the presence of HDAC inhibition; 4) whether the protective effects of HDAC inhibition were absent in the gp91^{phox}-deficient PLB-985 cells but present in wild-type cells; 5) whether disruption of gp-91 would mitigate the anti-apoptotic effect of HDAC inhibition in the *in vitro* cultured cells

exposed to simulated ischemia. To the best of our knowledge, this is the first study to provide new insight into our understanding of novel mechanisms of ischemic injury and developing therapeutic strategies for heart disease.

2. Materials and Methods

2.1. Animals

Adult male C57/BL6 wild-type and gp91$^{-/-}$ mice were supplied by Jackson laboratories (Bar Harbor, Maine). All animal experiments were conducted in accordance with the guidelines on humane use and care of laboratory animals for biomedical research published by the National Institutes of Health. The experimental protocol was approved and carried out in accordance with the guidelines adhered to the Institutional Animal Care and Use Committee.

2.2. Chemical supplies and antibodies

Trichostatin A was obtained from Calbiochem (San Diego, CA). N-(2-mercaptopropionyl)-gel electrophoresis supplies were obtained from BioRad Laboratories (Hercules, CA). The perfusion chemicals were purchased from Sigma (St. Louis, MO). Gp-91 polyclonal rabbit antibody, β-actin, gp-91 siRNA and negative control scrambled siRNA were purchased from Santa Cruz Biotechnology Inc. Mouse anti-sarcomeric actinin antibody was obtained from Sigma (St. Louis, MO). Anti-rabbit horseradish peroxidase-conjugated secondary antibody was purchased from Amersham (Piscataway, NJ).

2.3. Langendorff isolated heart perfusion

The methodology of Langendorff's isolated perfused heart preparation has been described previously in detail (26–29). Briefly, mice were anesthetized with an intraperitoneal injection (i.p.) of pentobarbital sodium (120 mg/kg). The hearts were rapidly excised and arrested in ice-cold Krebs-Henseleit buffer. They were then cannulated via the ascending aorta for retrograde perfusion by the Langendorff method using Krebs-Henseleit buffer containing (in mM) 110 NaCl, 4.7 KCl, 1.2 $MgSO_4$ $7H_2O$, 2.5 $CaCl_2$ $2H_2O$, 11 glucose, 1.2 KH_2PO_4, 25 $NaHCO_3$, and 0.5 EDTA. The buffer, aerated with 95% O_2:5% CO_2 to give a pH of 7.4 at 37°C, was perfused at a constant pressure of 55 mmHg. A water-filled latex balloon, attached to the tip of polyethylene tubing, was then inflated sufficiently to provide a left ventricular end-diastolic pressure (LVEDP) of 10 mmHg. Myocardial function was measured including left ventricular developed pressure (LVDP), LVEDP, RPP, heart rate and coronary flow. LVDP was calculated by subtracting LVEDP from the peak systolic pressure. Rate pressure product (RPP), an index of cardiac work, was calculated by multiplying LVDP with heart rate.

2.4 Measurement of myocardial infarction

The infarction size was measured with a modification as previously described (26–29). At the end of reperfusion, hearts were perfused with 10% triphenyltetrazolium chloride (TTC), and then removed from the Langendorff perfusion apparatus. The frozen hearts were then cut from apex to base into transverse slices. After staining, 10 % TTC buffer was replaced, and then the slices were fixed in formaldehyde for measurement of the infarcted areas using computer morphometry NIH image software (Image *J* 1. 36, NIH). The infarct size was calculated and presented as the percentage of risk area, defined as the sum of total ventricular area minus cavities.

2.5. Experimental protocol 1

Mice were randomized into three experimental groups that underwent the following treatments, as shown in Figure 1: 1) Vehicle group: wild-type mice receiving an i.p. injection of 0.1 ml vehicle (DMSO); 2) TSA+wild-type group: wild-type animals were treated the same as group

1 except that TSA (TSA, 0.1mg/kg, i.p.) was given to wild-type animals; 3) TSA+ gp-91$^{-/-}$ group: the same as group 2 except that mice with disruption of gp-91 was administered with TSA. Twenty-four hours later, the hearts were subjected to 30 min of stabilization and 30 min of ischemia followed by 30 min of reperfusion.

Another subset of animals without sustained ischemia and reperfusion was treated with or without TSA solely for the purpose of measuring the gp-91 protein. Animals were treated with TSA for 30 min, and heart tissues were collected. Cardiac lysates were extracted as previously described (37). Briefly, the hearts were frozen in liquid nitrogen, ground and suspended in 1 ml of lysis buffer containing 50 mM Tris HCl (pH 7.4), 0.1 mM sodium orthovanadate, 50 mM sodium fluoride, 150 mM sucrose, 1 mM phenylmethylsulfonyl fluoride (PMSF), 5 mM EDTA, 5 mM EGTA, 2 μg/ml leupeptin, 2 μg/ml aprotinin, and 5 μg/ml pepstatin A. Mixtures were homogenized and microcentrifuged at 16,000 × g for 20 min. The protein content of the supernatant was determined using the detergent compatible-protein assay (Bio-Rad). In addition, frozen hearts following treatments were used for the detection of ROS in cardiac sections.

2.6. Western blot analysis

The proteins were detected using polycolonal anti-gp-91, active caspase-3 from CalBiochem (San Diego, CA) and β-actin antibodies. For immunoblotting, proteins (50μg/lane) were separated by 6% SDS-PAGE (gp-91) and 10% SDS-PAGE (active caspase-3). Proteins were then transferred onto a nitrocellulose membrane for 2h at 100 Volts. The membrane was blocked with 5% non-fat dry milk in 1X Tris-buffered saline containing 0.5% Tween 20 for 1 h. The blots were incubated with respective primary antibodies (1:1,000 dilution) for 2 h and visualized by incubation with anti-rabbit horseradish peroxidase-conjugated secondary antibody (1:5,000 dilution) for 1 h. The immunoblots were developed with the ECL Chemiluminescence Detection Reagent (Amersham Pharmacia Biotech). The densitometric results were normalized to the control group and expressed as percentages of control values.

2.7. Cell culture and siRNA transfection

H9c2 cardiomyoblast cells, a clonal line derived from rat heart (ATCC, Rockville, MD), were grown in Dulbecco's modified Eagle's medium (DMEM) with 10% fetal calf serum, 100 units/ml penicillin and 0.1 mg/ml streptomycin. The siRNA transfections were done according to the description in the manufacturer’s protocol. The negative control (scrambled) siRNA and gp-91 siRNA were mixed with Lipofectamine™ 2000 (Invitrogen) at a final concentration at 500 nmol/L of siRNA in medium, respectively. At 24 hours of posttransfection, H9c2 cardiomyoblasts were subjected to simulated ischemia and reperfusion, which has been well-established in our laboratory.

2.8. Simulated ischemia

For simulated ischemic stress in cultured cells, the protocol for 30 minutes of ischemia and 30 minutes of reperfusion was carried out according to the experimental protocols 2 and 3. For TSA treatments, H9c2 cardiomyoblasts and PLB-985 cells were cultured in a 5% CO_2 at 37 °C and exposed to TSA (50 nmol/L) for 30 minutes before a subsequent 30 minutes of simulated ischemia was initiated. The SI medium was consisted of (mM): NaCl 115, KCl 5, KH_2PO_4 1, $MgSO_4$ 1.2, $CaCl_2$ $2H_2O$ and HEPES 25 containing 5 mM potassium cyanide (KCN) and 20 mM 2-deoxy-*D*-glucose. Cyanide treatment was terminated by rinsing twice with phosphate buffered saline (PBS). The medium was then replaced by DMEM for 30 minutes to mimic reperfusion. In order to elucidate the role of gp-91 in mediating TSA-induced cellular protection, it would be important to utilize the cell line that lacks of gp-91, which would provide us the genetic evidence to emphasize the relationship of gp91 and HDAC inhibition in the regulation of cellular response to stress stimulus. In this regard, we conducted another separate

experiment, in which gp91^{phox}-deficient PLB-985, PLB-985 wild-type cells were cultured as previously described (24,30). The execution of simulated ischemia and treatment of TSA were performed as described above. At the end of reperfusion, the cell viability and cell necrosis were evaluated. Gp91^{phox}-deficient PLB-985 and PLB-985 wild-type cells were obtained from Dr. Dinauer, M, Department of Pediatrics, Indiana University Medical Center, Indianapolis, Indiana.

2.9. Measurement of cell viability

The assessment of viabilities of H9c2 cardiomyocytes and PLB-985 cells was based upon the description and the principle of reduction of 3-[4,5-dimethylthiazol-2-yl]-2,5-diphenyl tetrazolium bromide (MTT) (St. Louis, MO) into blue formazan pigments in viable cells (31). At the end of the experiment, the medium was removed and the cells washed with PBS. MTT (0.01 g/ml) were dissolved in PBS, and 500 μl was added to each well. Cells were subsequently incubated for 2 h at 37 °C. Cells were then washed twice with PBS and 1 ml of HCl-isopropanol-Triton (1% HCl in isopropanol; 0.1% Triton X-100; 50:1) was added to each well for 5 minutes. The suspension was then centrifuged at 16,000 × g for 2 minutes. The optical density was determined spectrophotometrically at a wavelength of 540 nm and the values expressed as percentages of control values.

2.10. Measurements of cell necrosis

Loss of plasma membrane integrity (cell necrosis) was assessed by measuring the activity of LDH in the supernatant. A 100 μl supernatant was transferred into a 96-well plate. The release of lactate dehydrogenase (LDH) in the culture medium from H9c2 cardiomyoblast cells and PLB-985 cells at the end of reperfusion was determined as an indicator of cell necrosis using a commercially available kit (Roche), as per the manufacturer's protocol with a modification (32). The optical density was determined spectrophotometrically at a wavelength of 490nm and the values expressed as percentages of control values.

2.11. Detection of gp-91 and *in situ* production of superoxide in myocardium

For immunofluorescent staining, cardiac tissues were snap-frozen in melting 2-methylbutane and the 10 μm-thick sections were cut with a cryostat at −22−C and mounted on plus charge slides (Fisher Scientific). Sections were fixed in 3.7% (vol/vol) paraformaldehyde and then permeabilized in 0.5% Triton X-100 in PBS. The sections were then incubated for 30 minutes in 0.5% goat serum/0.2% (vol/vol) Tween 20 and subsequently incubated with the following primary antibodies for 1 h: a mouse monoclonal anti-sarcomeric actinin (1: 200 dilution) for recognizing myocytes and rabbit polyclonal gp-91 for detecting the gp-91. After three 5 minute washings in PBS, the following secondary antibodies were applied: fluorescein goat anti-rabbit IgG (H+L) for rabbit polyclonal gp-91 and Texas red horse anti-mouse IgG (H+L) for sarcomeric actinin. Nuclei were stained with 4'-6-Diamidino-2-phenylindole (DAPI) at a concentration of 10 μg/ml. In situ detection of superoxide was performed as described previously (33). Briefly, slides were placed into PBS for 30 min at room temperature and then stained with dihydroethidium (DHE, 10μM) in PBS for 60 min in a moist chamber in the dark. The slides were rinsed extensively with PBS and then coverslipped. Fluorescent imaging was performed with a Nikon E2000 fluorescence microscope, equipped with MetaVue software for image analysis.

2.12. Statistics

All measurements are expressed as means ± SE. Difference among the groups were analyzed by one-way analysis of variance (ANOVA), followed by post hoc Bonferroni correction or Student's unpaired *t* test for two groups. Statistical differences were considered significant with a value of $p<0.05$.

3. Results

3.1 Myocardial functional recovery of HDAC inhibition depends on gp-91

Baseline ventricular function including LVSP, LVEDP, LVDP, rate pressure product, and heart rate, were recorded among the groups. There were no differences among the groups before ischemia. As shown in Figure 2, compared to the vehicle-treated animals, the treatment of mice with TSA, resulted in a profound improvement in post-ischemic left ventricular functional recovery in left ventricular end-diastolic pressure. TSA-induced post-ischemic improvement in LVEDP was abrogated in animals with disruption of the gp-91 subunit of NADPH-oxidase ($p< 0.05$, Fig. 2A). In addition, the recovery of the RPP reached a marginal improvement following TSA treatment as compared to vehicle-treated group (Fig. 2B). Similarly, disruption of the gp-91 subunit of NADPH-oxidase abolished the recovery of rate pressure product. Although TSA treatment in wild-type mice demonstrated a mild increase in coronary effluent, however, there were no significant differences in the heart rate and coronary flow among groups following ischemia and reperfusion (Fig. 2C, 2D).

3.2. Disruption of gp-91 abolishes the infarct-sparing effect of HDAC inhibition

Myocardial infarct size, an index of irreversible myocardial injury, was measured. The infarct size in the vehicle group was 33.0 ± 3 %. However, the infarct size in the TSA treated group was reduced to 9.6 ± 2 %, but the infarct-sparing effect following TSA treatment was increased to 27 ± 1 % ($p<0.001$, Figure 3). The data suggest that the reduction of infarct size by HDAC inhibition is closely related with gp-91 subunit of NADPH-oxidase subunit.

3.3. HDAC inhibition increases gp-91 and *in situ* ROS production

We examined the effect of TSA treatment on gp-91 content. As shown in Figure 4A, gp-91 was detectable in the myocardium from control animals, and densitometric analysis demonstrates that TSA treatment caused a remarkable increase in gp-91. There was no significant change in β actin, indicating a gp-91 subunit of NADPH-oxidase subunit was augmented following an increase of hyperacetylation. In addition, as shown in Figure 4C, immunofluorescent staining shows an increase in gp-91 signals following HDAC inhibition as compared to the vehicle group. Furthermore, the detection of superoxide with dihydroethidium staining indicates that TSA treatment increased the production of superoxides (Figure 5A–C).

3.4. HDAC inhibition increases the cell survival through gp-91

As shown in Figure 6A, western blot shows a reduction in expression of gp-91 in H9c2 cardiomyoblast cells transfected with gp-91 siRNA but not scrambled siRNA. This suggests that siRNA silencing effectively knocked down gp-91 expression of H9c2 cadiomyoblasts. As shown in Figure 6B, simulated ischemic stimulus led to an increase of intracellular LDH leakage as compared to the control, which significantly decreased by pre-treatment of H9c2 cells with 50 nmol/L of TSA. However, genetic knockdown of gp-91 with siRNA remarkably prevented the reduction of LDH leakage from HDAC inhibition, but the scrambled siRNA did not exhibit effect of HDAC inhibition on LDH. Furthermore, simulated ischemia decreased cell viability, which was profoundly prevented by HDAC inhibition. The improvement in cell viability of HDAC inhibition was also absent by the knockdown of gp-91 with specific siRNA (Figure 6C). To further confirm the protective effect of gp-91 on necrosis and viability, well-established gp-91 genetic mutant cells were tested for their tolerance to ischemic stress. As shown in Figure 7A and B, simulated ischemic stimulus increased the necrosis and decreased the cell viability of PLB-985 wild-type cells, but TSA treatment enhanced the resistance of cells to simulated ischemia, as indicated by the increase in cell viability and reduction of LDH leakage. These protective effects of TSA on wildtype PLB-985 cells were absent in the

gp91^{phox}-deficient PLB-985 cells. Thus, this data suggests that gp-91 contributes to the HDAC inhibition-induced protection.

3.5. HDAC inhibition reduces apoptosis

We next examined whether HDAC inhibition through gp-91 affects programmed cell death. We focused on assessing apoptosis by measuring the appearance of active caspases, because apoptotic stimuli activate the caspase cascade and the final cleaved forms of effector caspases, such as caspase-3, then cleave substrates important in the maintenance of cellular integrity. As shown in Figure 8A and B, there was active caspase-3 in H9c2 cardiomyoblasts exposed to simulated ischemia stress. However, TSA treatment significantly reduced the content of active caspase-3, which was prevented by genetic silencing of gp-91, but not scrambled siRNA ($p<0.05$). Furthermore, as shown in Figure 8C and D, there was an increase in active caspase-3 in both wild-type and gp91^{phox}-deficient PLB-985 cells exposed to simulated ischemia as compared to the control group. However, TSA treatment decreased the caspase-3 content in wild-type cells ($p<0.05$), but not in gp91^{phox}-deficient PLB-985 cells. The caspase-3 contents in gp-91^{phox}-deficient PLB-985 cells were also higher than that of wild-type cells exposed to SI in the presence of TSA. Collectively, the results indicate that gp-91 can mediate the effects of HDAC inhibition through inhibiting a well-characterized apoptotic pathway.

4. Discussion

Salient findings

The growing evidence indicates HDAC inhibition as a novel signaling pathway to confer myocardial protection following I/R. The molecular signaling event that underlies the HDAC inhibition-induced protective effect remains unknown. In this investigation, we have demonstrated that the genetic deletion of gp91 abrogated myocardial protection of HDAC inhibition. The inhibition of HDAC resulted in an increase in gp-91 protein, which was associated with a mild increase of superoxide. Using interfering siRNA and well-established cell culture models, we found that HDAC inhibition increased the resistance of H9c2 cardiomyoblasts to simulated ischemia, which was indicated by the reduction of cell necrosis and improvement in cell viability. The beneficial effects of HDAC inhibition on cell viability and necrosis were mitigated with genetic suppression of the gp-91 with siRNA. Furthermore, stimulation of PLB-985 cells with TSA prevented the cell necrosis and enhanced the cell viability, which were absent in the gp91^{phox}-deficient PLB-985 cells that lack the gp-91. TSA also shows the inhibition of cleaved caspase 3 protein, anti-apoptotic effect of HDAC inhibition was blocked with genetic knockdown of gp-91. Taken together, this study is the first demonstration to reveal that gp-91 subunit of NADPH-oxidase constitutes a novel major pathway of HDAC inhibition to confer cardioprotection.

The class II HDACs are abundantly expressed in the heart (7,10). TSA was originally isolated from *Streptomyces hygroscopicus* and acts as a potent inhibitor of HDAC (34). TSA binds to the deacetylase catalytic core to form a tubular pocket, a zinc-binding site, and two Asp-His charge-relay system to inhibit the histone acetylase (35). In this study, we used TSA at 50 nmol/L to inhibit HDAC activity, which produced the cardioprotective effect and a significant increase in acetylated histone 4 in hearts (12,13), suggesting the potency of acetylation by HDAC inhibitor and providing a basis of TSA employed in our study. The treatment of the heart with TSA caused an improvement in ventricular functional recovery in post-ischemic heart and the reduction of myocardial infarct size (12). This is consistent with previous observations in which either inhibition of HDAC activity or knockdown of a specific HDAC reduces infarct size and/or prevents cellular injury (36). Furthermore, the protective effects of HDAC inhibition have also been reported in hypertrophic mice models, and cardiomyocytes (14,15,37). Even though these observations have characterized HDAC inhibition as a common

pathway to orchestrate myocardial protection, the mechanism by which HDAC inhibitors confers cardioprotection is still poorly understood. Interestingly, these beneficial effects of HDAC inhibition on the improvement of ventricular function and reduction of infarct size in the wild-type were abrogated in mice with disruption of the gp-91 subunit of NADPH-oxidase. These evidences suggest that HDAC inhibition mediates the cardioprotection via gp-91 of NADPH-oxidase. In addition, another observation indicates that mice with an ablation of gp-91 show a slight lower systolic pressure, which is attributable to vascular smooth muscle tone (38). However, we have not demonstrated a significant difference in cardiac function in normal condition, it might be possible that gp-91 differently mediates myocardial and vascular phenotypes. Some discrepancies may also be related to the different models used.

Previous studies have well documented that the mild production of ROS plays a pivotal role in initiating preconditioning effect which protects the heart against ischemic injury (39–43). The protective effects of ROS in the preconditioned hearts are demonstrated to involve the activation of the mitochondrial K_{ATP} channel and transcriptional factor NF-κB, which constitute the most robust signaling pathway against ischemia and reperfusion injury. In addition, our previous works have already suggested that administration of an inhibitor of nitric oxide markedly attenuated myocardial protection by the activation of adenosine receptor A3 (27). Considerable observations indicate that the production of mild ROS is one of the important mechanism(s) in development of cardioprotection, whereas $gp91^{phox}$ subunit is centrally involved in the generation of ROS in NADPH oxidase. In addition to the fact that the $gp91^{phox}$ was mostly confined to vascular smooth muscles and endothelial cells in myocardium (44), we have shown the presence of gp-91 in mouse myocardium, providing a basis for us to investigate gp-91 in the ischemic heart (20). The mechanism by which gp-91 was increased following HDAC inhibition is not clear. It will be interesting to elucidate whether the mediation of gp-91 with HDAC inhibition is associated with transcriptional regulation or protein degradation.

Whether HDAC inhibition couples with gp-91 in the genesis of cardioprotection, has never been tested. However, HDAC inhibitor, MS-275 potently induced an increase in reactive oxygen species in U937 cells, followed by the loss of mitochondrial membrane potential (25). This is consistent with the observation that HDAC inhibition mediated cytotoxic effect via reactive oxidant species in nonproliferating chronic lymphocytic leukemia. Despite the plethora of evidence showing a potential link between the HDAC inhibition and production of ROS, there was no study reporting a cascade consisting of HDAC inhibition and gp-91 and their functional coupling. The loss of protective effects of HDAC inhibition in $gp\text{-}91^{-/-}$ mice suggests the importance of this working module in the ischemic heart. H9c2 cardiomyoblast cells have been widely used as a powerful *in vitro* model to study I/R injury (44). Using the *in vitro* H9c2 myocytes, we conducted the experiment of the simulated ischemia, which is a well-established approach to study cellular injury (31,44). Treatment of H9c2 cardiomyoblast cells with the HDAC inhibitor augmented the resistance to simulated ischemia by enhancing cell viability and decreasing the cell necrosis. However, these protective effects totally diminished in cells transfected with interfering siRNA to knockdown the gp91 subunit. Furthermore, this observation was further confirmed by the employed study in which the enhanced resistance of wild-type cells to simulated ischemia by HDAC inhibition was lost in $gp91^{phox}$-deficient PLB-985. In other observations using different model and cell lines, HDAC inhibition has shown to be pro-apoptosis and the sustained administration of angiotensin II induced a gp-91 dependent hypertrophic heart failure (45). The reasons for these discrepancies are unclear, but it is likely to be related to different responses in different models and the strength of gp-91 activation. In the present study, we do not investigate whether other cytosolic subunits of NADPH-oxidases were also involved in HDAC inhibition-induced cardioprotection. This is a subject matter which merits further investigation.

In summary: In the present investigation, we have revealed a novel mechanism by which the activation of gp-91, a subunit of NADPH-oxidase following HDAC inhibition is essential to induce cardioprotection. HDAC inhibition caused an increase of gp-91 in the myocardium, which led to a subsequent production of reactive oxidant species. These data suggest a direct cause and effect relationship between HDAC inhibition and gp-91 activation which orchestrates cardioprotection. We have proven the central role of this novel pathway by demonstrating the abrogation of cardioprotection by the targeted deletion of gp-91 in mice. Furthermore, using *in vitro* H9c2 cardiomyoblast culture, siRNA gene silencing, as well as gp91^{phox}-deficient cells, we show evidence that the reduction of cell necrosis and increase in viability following HDAC inhibition were mitigated with genetic knockdown or deletion of gp-91. Furthermore, HDAC inhibition increased the anti-apoptotic effects in cultured cells exposed to simulated ischemia. To the best of our knowledge, this is the first study providing direct evidence of mediating gp-91 by HDAC inhibition to induce cardioprotective effects. Our investigation not only provides new insight into our understanding of mechanisms of myocardial I/R, but also suggests that therapeutic strategies targeting this signaling pathway could be a novel and useful approach to the protection of the ischemic myocardium.

Acknowledgments

The work is supported by the National Heart, Lung, and Blood Institute Grant (R01 HL089405) and American Heart Association-National center (0735458N) to TCZ.

References

1. Cheung P, Allis CD, Sassone-Corsi P. Signaling to chromatin through histone modifications. Cell 2000;103:263–267. [PubMed: 11057899]
2. Hansen JC, Tse C, Wolffe AP. Structure and function of the core histone N-termini: more than meets the eye. Biochemistry 1998;37 17637-4.
3. Luger K, Mader AW, Richmond RK, Sargent DF, Richmond TJ. Crystal structure of the nucleosome core particle at 2.8 A resolution. Nature 1997;389:251–260. [PubMed: 9305837]
4. Strahl BD, Allis CD. The language of covalent histone modifications. Nature 2000;403:41–45. [PubMed: 10638745]
5. Turner BM. Histone acetylation and an epigenetic code. Bioessays 2000;22:836–845. [PubMed: 10944586]
6. Hassig CA, Tong JK, Fleischer TC, Owa T, Grable PG, Ayer DE, Schreiber SL. A role for histone deacetylase activity in HDAC1-mediated transcriptional repression. Proc Natl Acad Sci U S A 1998;95:3519–3524. [PubMed: 9520398]
7. Verdin E, Dequiedt F, Kasler HG. Class II histone deacetylases: versatile regulators. TRENDS in Genetics 2003;19:286–293. [PubMed: 12711221]
8. Fischle W, Emiliani S, Hendzel MJ, Nagase T, Nomura N, Voelter W, Verdin E. A new family of human histone deacetylases related to Saccharomyces cerevisiae HDA1. Biol Chem 1999;274:11713–11720.
9. Grozinger CM, Hassig CA, Schreiber SL. Three proteins define a class of human histone deacetylases related to yeast Hda1p. Proc Natl Acad Sci U S A 1999;96:4868–4873. [PubMed: 10220385]
10. Wang AH, Bertos NR, Vezmar M, Pelletier N, Crosato M, Heng HH, Th'ng J, Han J, Yang XJ. HDAC4, a human histone deacetylase related to yeast HDA1, is a transcriptional corepressor. Mol Cell Biol 1999;19:7816–7827. [PubMed: 10523670]
11. Vigushi DM, Coombes RC. Targeted histone deacetylase inhibition for cancer therapy. Current Cancer Target 2004;4:205–218.
12. Zhao TC, Cheng G, Zhang LX, Tseng YT, Padbury JF. Inhibition of histone deacetylases triggers pharmacologic preconditioning effects against myocardial ischemic injury. Cardiovasc Res 2007;76:473–481. [PubMed: 17884027]

13. Antos CL, McKinsey TA, Dreitz M, Hollingsworth LM, Zhang CL, Schreiber K, Rindt Qian YRH, Gorczynski RJ, Olson EN. Dose-dependent blockade to cardiomyocyte hypertrophy by histone deacetylase inhibitors. J Biol Chem 2003;278:28930–28937. [PubMed: 12761226]
14. Kee HJ, Sohn IS, Nam KI, Park JE, Yin Z, Ahn Y, Jeong MH, Bang YJ, Kim N, Kim JK, Kim KK, Epstein JA, Kook H. Inhibition of histone deacetylation blocks cardiac hypertrophy induced by angiotensin II infusion and aortic banding. Circulation 2006;113:51–59. [PubMed: 16380549]
15. Kong Y, Tannous P, Lu G, Berenji K, Rothermel BA, Olson EN, Hill JA. Suppression of class I and II histone deacetylases blunts pressure-overload cardiac hypertrophy. Circulation 2006;113:2579–2588. [PubMed: 16735673]
16. Ren M, Leng Y, Jeong M, Leeds PR, Chuang DM. Valproic acid reduces brain damage induced by transient focal cerebral ischemia in rats: potential roles of histone deacetylase inhibition and heat shock protein induction. J Neurochem 2004;89:1358–1367. [PubMed: 15189338]
17. Leto, TL. inflammation Basic and Clinical Correlates. Gallin, JI.; Snyderman, R., editors. Lippincott, Wilkins, Philadelphia: 1999. p. 769-787.
18. dler V, Yin Z, Tew KD, Ronai Z. Role of redox potential and reactive oxygen species in stress signaling. Oncogene 1999;18:6104–6111. [PubMed: 10557101]
19. Ebert BL, Bunn HF. Regulation of the erythropoietin gene. Blood 1999;94:1864–1877. [PubMed: 10477715]
20. Zhao TC, Kukreja RC. Reactive oxygen species and adenosine A_3 receptor induced delayed cardioprotection in mouse heart: essential role of gp91 subunit of NADPH oxidase. Circulation 2002;106:II–314.
21. Gorlach A, Brandes RP, Nguyen K, Amidi M, Dehghani F, Busse R. A $gp91^{phox}$-containing NADPH oxidase selectively expressed in endothelial cells is a major source of oxygen radical generation in the arterial wall. Circ Res 2000;87:26–32. [PubMed: 10884368]
22. Bayraktutan U, Blayney L, Shah AM. Molecular characterization and localization of the NAD(P)H oxidase components gp91-phox and p22-phox in endothelial cells. Arterioscler Thromb Vasc Biol 2000;20:1903–1911. [PubMed: 10938010]
23. Ushio-Fukai M, Zafari AM, Fukui T, Ishizaka N, Griendling KK. $p22^{phox}$ is a critical component of the superoxide-generating NADH/NADPH oxidase system and regulates angiotensin II-induced hypertrophy in vascular smooth muscle cells. J Biol Chem 1996;271:23317–23321. [PubMed: 8798532]
24. Bjorgvinsdottir H, Zhen L, Dinauer M. Cloning of murine gp-91 phox cDNA and functional analysis in a human X-linked chronic granulomatous disease cell line. Blood 1996;87:2005–2010. [PubMed: 8634451]
25. Dai Y, Rahmani M, Dent P, Grant S. Blockade of histone deacetylase inhibitor-induced RelA/p65 acetylation and NF-kappaB activation potentiates apoptosis in leukemia cells through a process mediated by oxidative damage, XIAP downregulation, and c-Jun N-terminal kinase 1 activation. Mol Cell Biol 2005;25:5429–5444. [PubMed: 15964800]
26. Zhao T, Parikh P, Bhashyam S, Bolukoglu H, Poornima I, Shen YT, Shannon RP. Direct effects of glucagon-like peptide-1 on myocardial contractility and glucose uptake in normal and postischemic isolated rat hearts. J Pharmacol Exp Ther 2006;317:1106–1113. [PubMed: 16489128]
27. Zhao TC, Kukreja RC. Late preconditioning elicited by activation of adenosine A(3) receptor in heart: role of NF- kappa B, iNOS and mitochondrial K(ATP) channel. J Mol Cell Cardiol 2002;34:263–277. [PubMed: 11945020]
28. Zhao TC, Kukreja RC. Protein kinase C-delta mediates adenosine A3 receptor-induced delayed cardioprotection in mouse. Am J Physiol Heart Circ Physiol 2003;285:H434–H441. [PubMed: 12793983]
29. Zhao TC, Taher MM, Valerie KC, Kukreja RC. p38 Triggers late preconditioning elicited by anisomycin in heart: involvement of NF-kappaB and iNOS. Circ Res 2001;89:915–922. [PubMed: 11701619]
30. Zhen L, King AA, Xiao Y, Chanock SJ, Orkin SH, Dinauer MC. Gene targeting of X chromosome-linked chronic granulomatous disease locus in a human myeloid leukemia cell line and rescue by expression of recombinant gp91phox. Proc Natl Acad Sci U S A 1993;90:9832–9836. [PubMed: 8234321]

31. Engelbrecht AM, Niesler C, Page C, Lochner A. p38 and JNK have distinct regulatory functions on the development of apoptosis during simulated ischaemia and reperfusion in neonatal cardiomyocytes. Basic Res Cardiol 2004;99:338–350. [PubMed: 15309413]
32. Tantini B, Fiumana E, Cetrullo S, Pignatti C, Bonavita F, Shantz LM, Giordano E, Muscari C, Flamigni F, Guarnieri C, Stefanelli C, Caldarera CM. Involvement of polyamines in apoptosis of cardiac myoblasts in a model of simulated ischemia. J Mol Cell Cardiol 2006;40:775–782. [PubMed: 16678846]
33. Li M, Dai X, Watts S, Kreulen D, Fink G. Increased superoxide levels in ganglia and sympathoexcitation are involved in sarafotoxin 6c-induced hypertension. Am J Physiol Regul Integr Comp Physiol 2008;295:R1546–R1554. [PubMed: 18768769]
34. Yoshida M, Kijima M, Akita M, Beppu T. Potent and specific inhibition of mammalian histone deacetylase both in vivo and in vitro by trichostatin A. J Biol Chem 1990;265:17174–17179. [PubMed: 2211619]
35. Finnin MS, Donigian JR, Cohen A, Richon VM, Rifkind RA, Marks PA, Breslow R, Pavletich NP. Structures of a histone deacetylase homologue bound to the TSA and SAHA inhibitors. Nature 1999;401:188–193. [PubMed: 10490031]
36. Granger A, Abdullah I, Huebner F, Stout A, Wang T, Huebner T, Epstein JA, Gruber PJ. Histone deacetylase inhibition reduces myocardial ischemia-reperfusion injury in mice. FASEB J 2008;22:3549–3560. [PubMed: 18606865]
37. Gallo P, Latronico MV, Gallo P, Grimaldi S, Borgia F, Todaro M, Jones P, Gallinari P, De Francesco R, Ciliberto G, Steinkühler C, Esposito G, Condorelli G. Inhibition of class I histone deacetylase with an apicidin derivative prevents cardiac hypertrophy and failure. Cardiovasc Res 2008;80:416–424. [PubMed: 18697792]
38. Wang HD, Xu S, Johns DG, Du Y, Quinn MT, Cayatte AJ, Cohen RA. Role of NADPH oxidase in the vascular hypertrophic and oxidative stress response to angiotensin II in mice. Circ Res 2001;88:947–953. [PubMed: 11349005]
39. Peart JN, Gross GJ. Cardioprotection following adenosine kinase inhibition in rat hearts. Basic Res Cardiol 2005;100:328–336. [PubMed: 15795795]
40. Sun JZ, Tang XL, Park SW, Qiu Y, Turrens JF, Bolli R. Evidence for an essential role of reactive oxygen species in the genesis of late preconditioning against myocardial stunning in conscious pigs. J Clin Invest 1996;97:562–576. [PubMed: 8567981]
41. Oldenburg O, Cohen MV, Yellon DM, Downey JM. Mitochondrial K(ATP) channels: role in cardioprotection. Cardiovasc Res 2002;55:429–437. [PubMed: 12160940]
42. Heinzel FR, Luo Y, Li X, Boengler K, Buechert A, García-Dorado D, Di Lisa F, Schulz R, Heusch G. Impairment of diazoxide-induced formation of reactive oxygen species and loss of cardioprotection in connexin 43 deficient mice. Circ Res 2005;97:583–586. [PubMed: 16100048]
43. Sun HY, Wang NP, Kerendi F, Halkos M, Kin H, Guyton RA, Vinten-Johansen J, Zhao ZQ. Hypoxic postconditioning reduces cardiomyocyte loss by inhibiting ROS generation and intracellular Ca2+ overload. Am J Physiol Heart Circ Physiol 2005;288:H1900–H1908. [PubMed: 15563525]
44. Geiszt M, Kopp JB, Varnal P, Leto TL. Identification of Renox, and NAD(P)H oxidase in kidney. Proc Natl Acad Sci USA 2000;97:8010–8014. [PubMed: 10869423]
45. Vitadello M, Penzo D, Petronilli V, Michieli G, Gomirato S, Menabò R, Di Lisa F, Gorza L. Overexpression of the stress protein Grp94 reduces cardiomyocyte necrosis due to calcium overload and simulated ischemia. FASEB J 2003;17:923–925. [PubMed: 12670879]
46. Bendall JK, Cave AC, Heymes C, Gall N, Shah AM. Pivotal role of a gp91(phox)-containing NADPH oxidase in angiotensin II-induced cardiac hypertrophy in mice. Circulation 2002;105:293–296. [PubMed: 11804982]

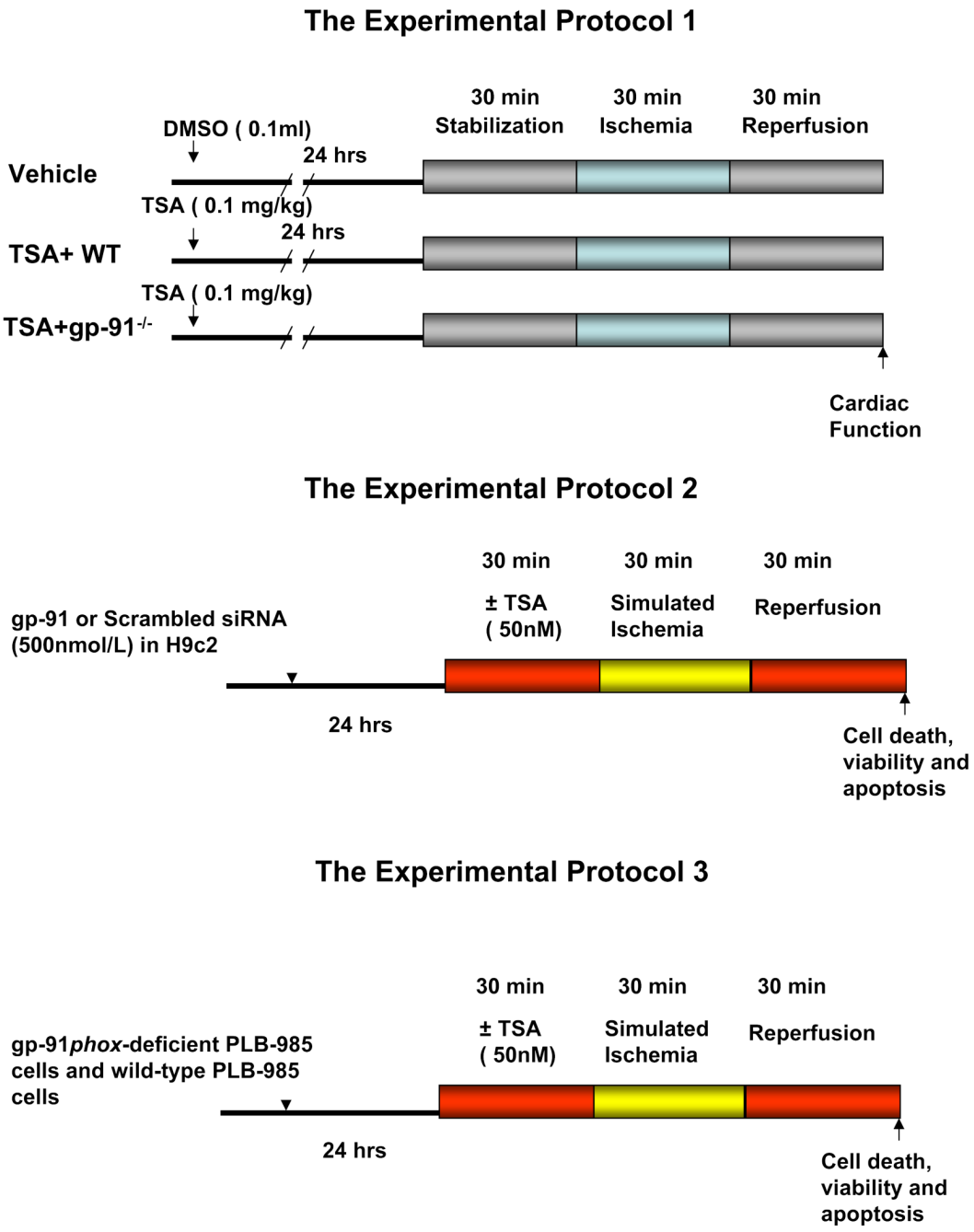

Figure 1.
Experimental protocols. See Methods for the groups and treatments.

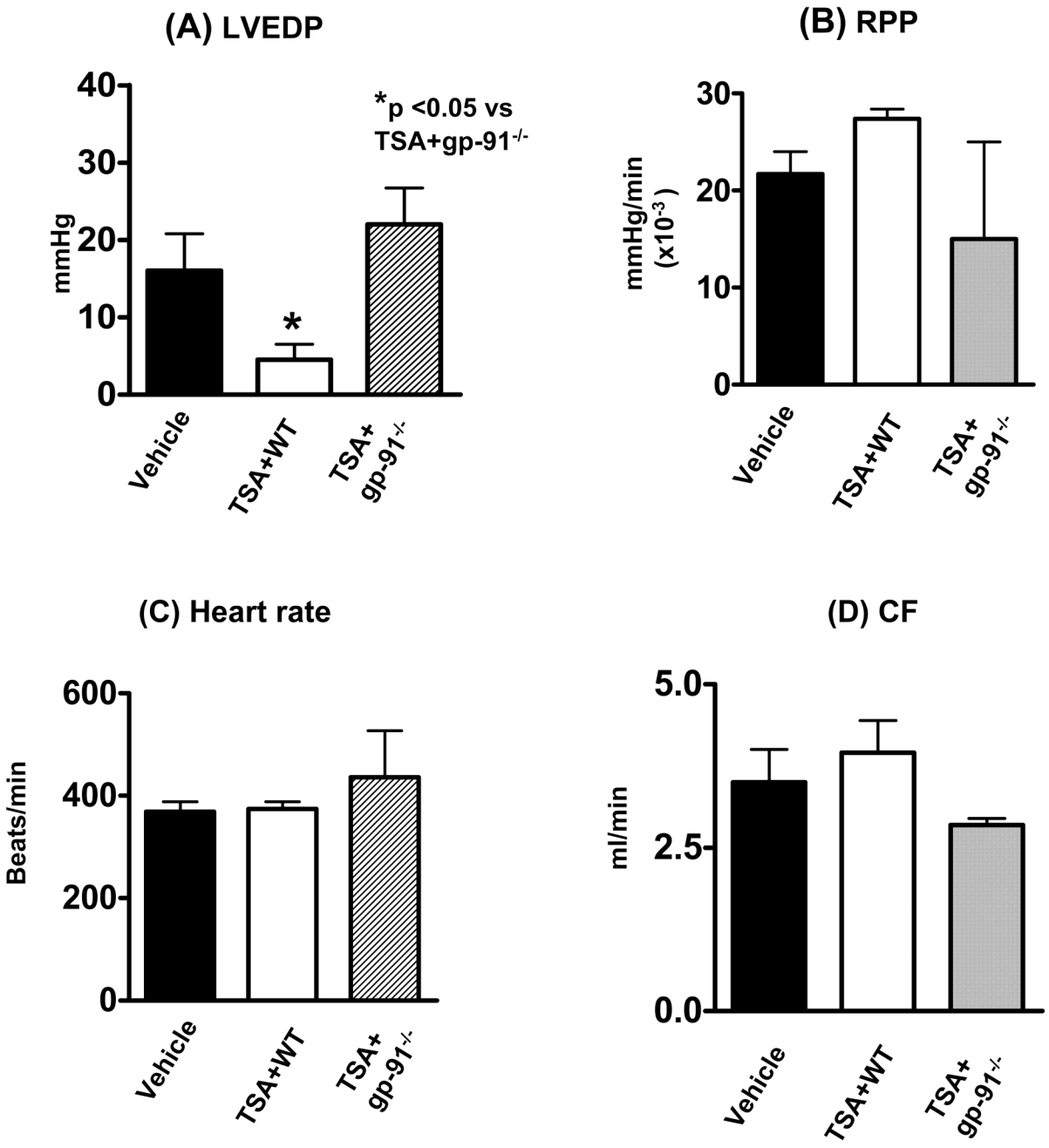

Figure 2.

Effect of TSA on post-ischemic ventricular function in wild-type and gp91 $^{-/-}$ mice. (A): left ventricular end-diastolic pressure (LVEDP); (B): Rate pressure product (RPP); (C): Heart rate (HR) and (D): Coronary effluent (CF). TSA: trichostatin A; Values represent means ± SE (n=4–6/group). *p<0.05.

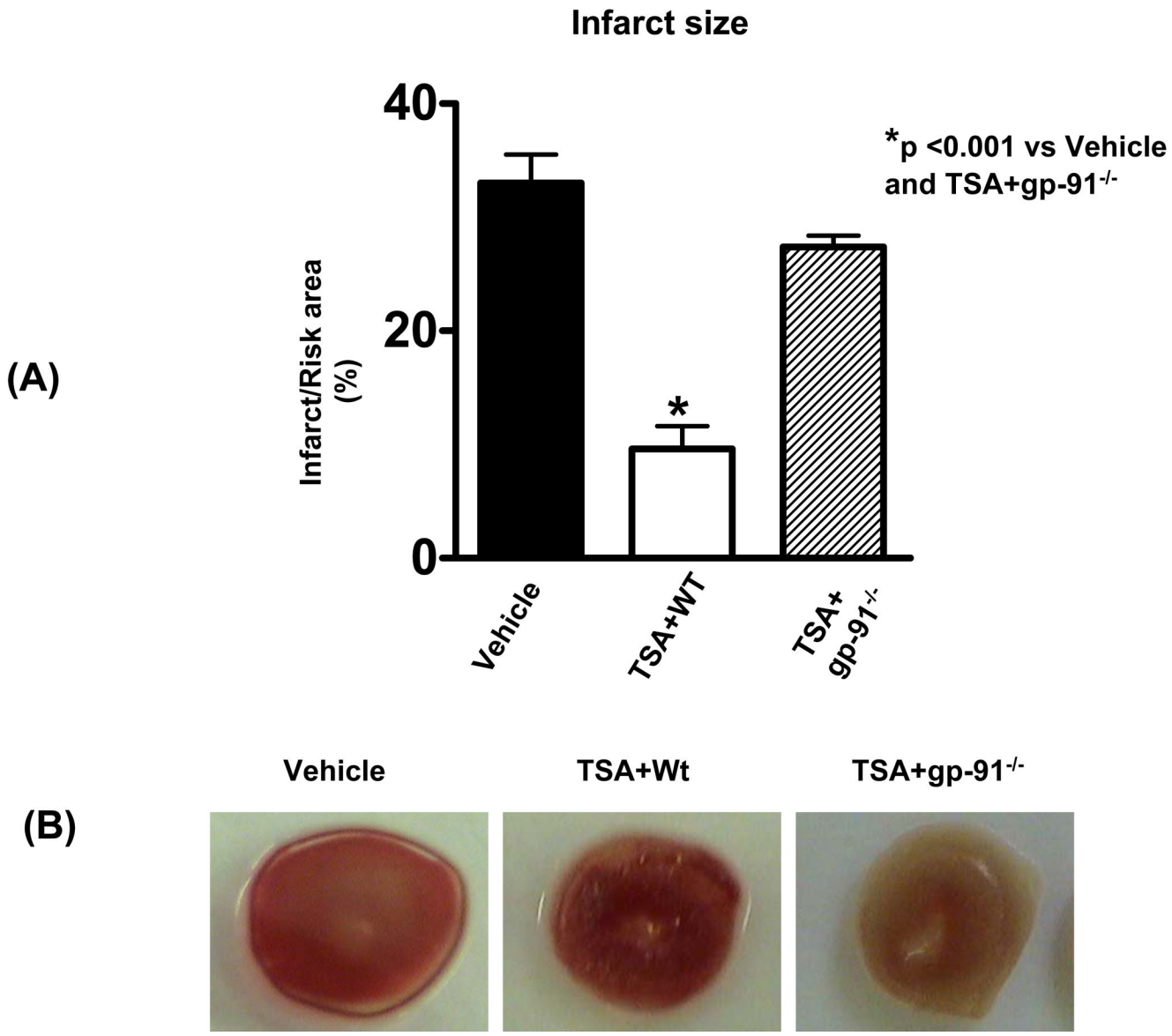

Figure 3.

The effect of TSA on infarct size in wild-type and gp-91$^{-/-}$ mice (A) and representative infarct image from each group (B). At the end of experimental protocol as described in METHODS, the hearts were stained with 2,3,5-triphenyltetrazolium chloride followed by fixation in formalin. Viable areas are stained brick red, whereas infarcted are gray or white. TSA: trichostatin A. Values represent means ± SE (n=4–7). *p<0.001.

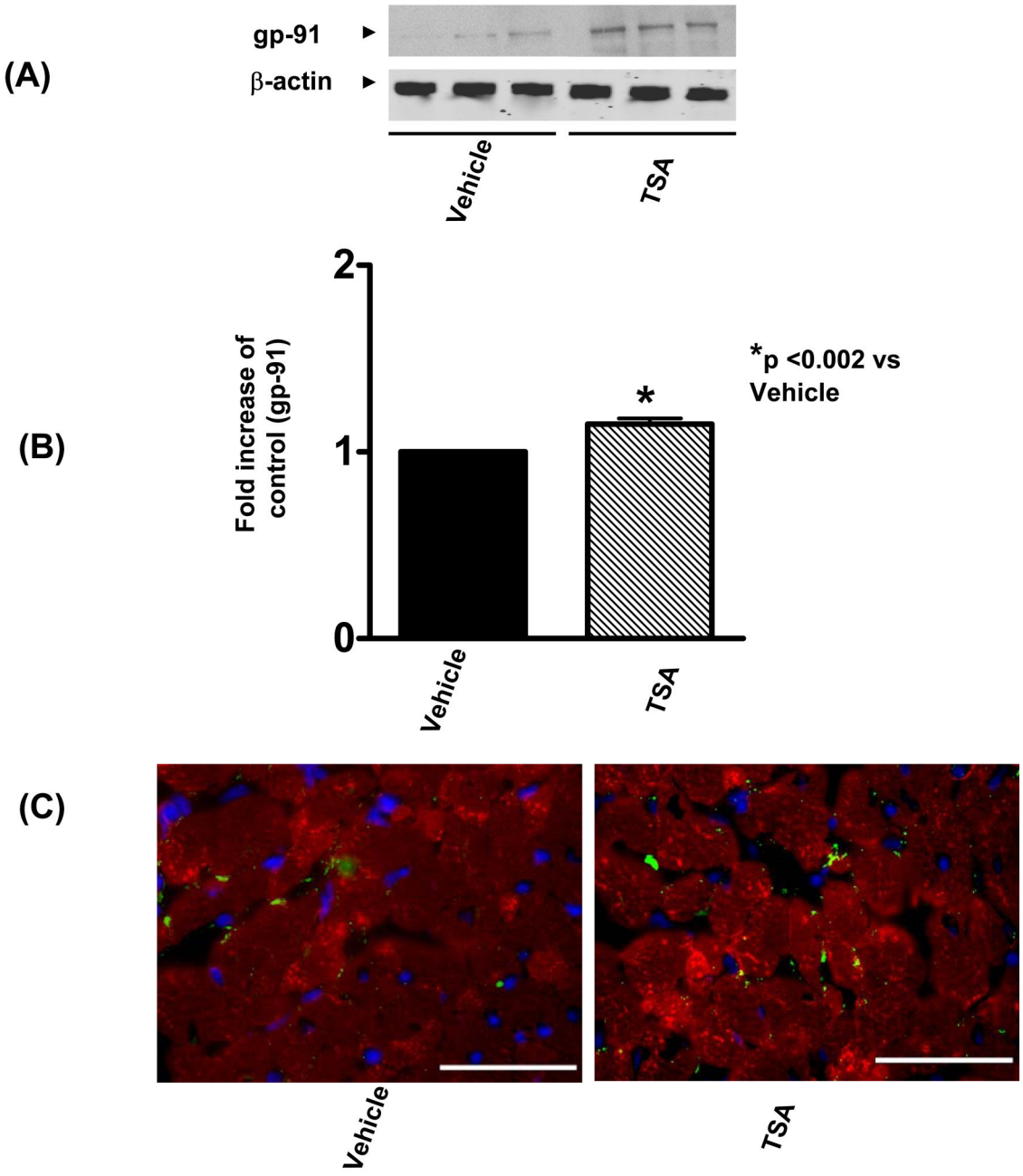

Figure 4.

(A): Representative Western blot showing the effect of TSA on gp-91 in the myocardium. (B): Quantification of gp-91 in the myocardium after TSA stimulation. The densitometric signal was normalized to the vehicle group and expressed as a percentage. Results are means ± SE (n=3/group), *P<0.002 vs vehicle. (C): the myocytes were stained with anti-sarcomeric actinin (red), gp-91 proteins were stained with anti-gp-91 (green). Nuclei were stained with 4'6-diamidino-2-phenylindole (DAPI, blue). Images show an overlay of myocytes, gp-91 and nuclei. Left panel represents vehicle-treated group and right panel represents TSA-treated hearts. Bar =50μm.

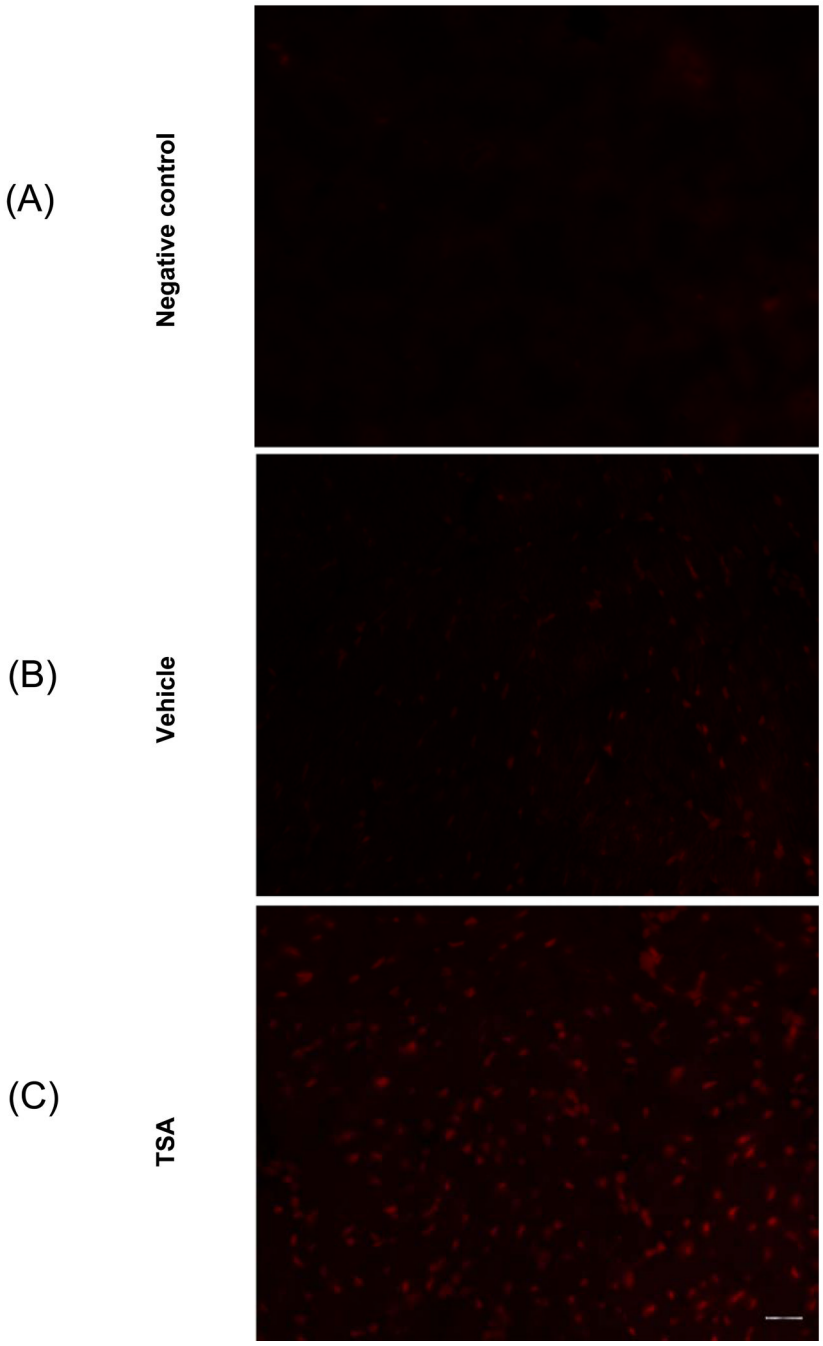

Figure 5.
Dihydroethidium (DHE) fluorescence detection of ROS production in cardiac sections. Cardiac sections from vehicle-treated and TSA treated hearts were incubated with 10μM of DHE. The DHE fluorescences were visualized under microscopy. (A): Negative control (without DHE incubation); (B): Vehicle-treated hearts; (C): TSA-treated hearts. Bar =50μm.

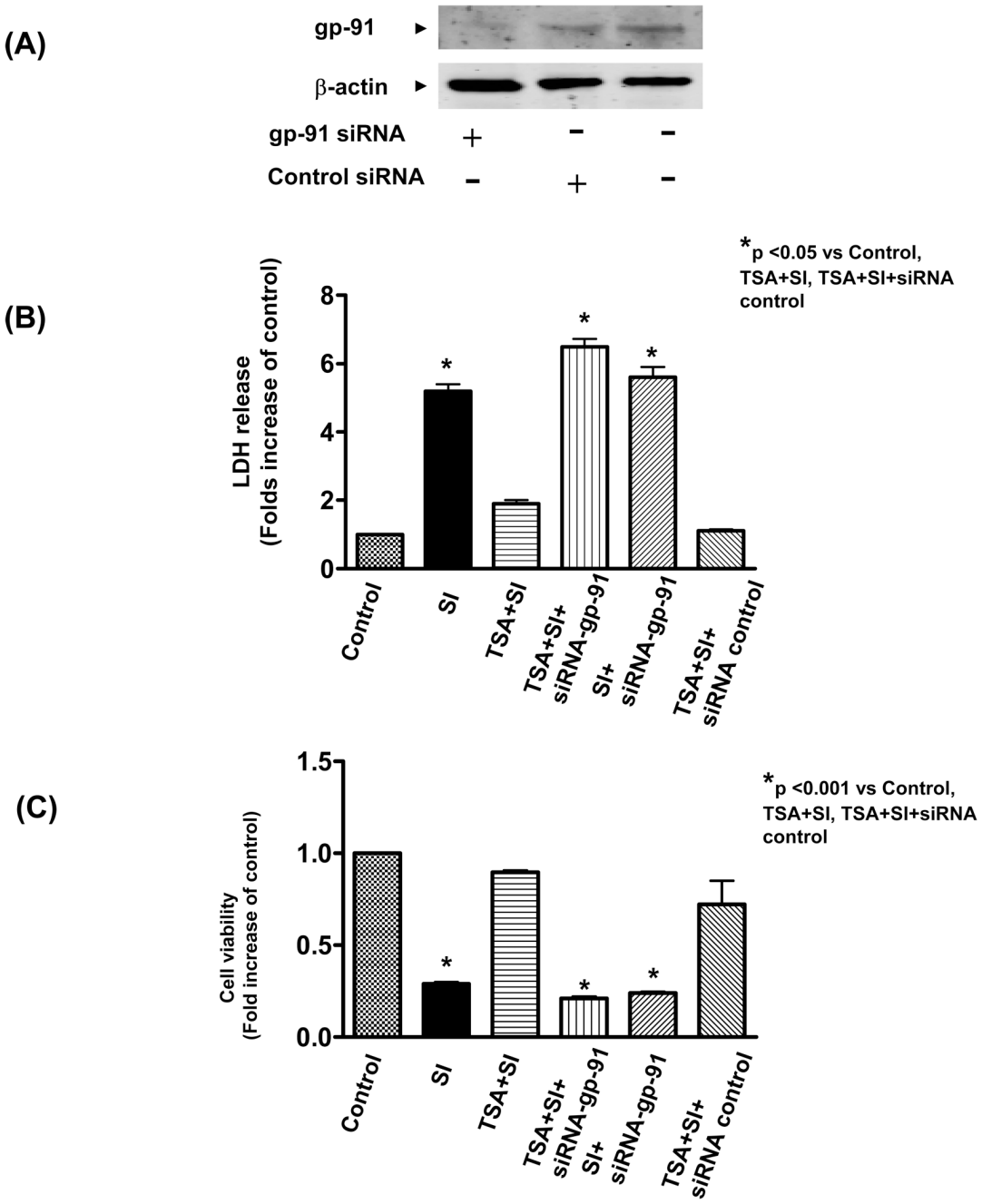

Figure 6.

Western blot analysis of gp-91 in H9c2 cardiomyoblasts transfected with or without gp-91 siRNA. (A): H9c2 cardiomyoblast were transfected with gp-91 (500 nmol/L) or scrambled siRNA (500 nmol/L) for 24 h to prepare protein lysates and following immunoblotting assay. (B) The LDH release of H9c2 myocytes in culture medium at the end of reperfusion (n=4/group). (C): Cell viability was measured using the MTT cell viability assay (n=4/group). H9c2 cardiomyoblast cells were exposed to simulated ischemia (KCN and 2-deoxy-D-glucose) and description of simulated ischemia is provided under METHODS. HDAC inhibitor, trichostatin A (50 nmol/L) was maintained in culture medium. Gp-91 and negative control siRNA transfections are described as under METHODS. SI: simulated ischemia. LDH: lactate

dehydrogenase. Results are expressed as means ± SE and the values expressed as percentages of control values. *P < 0.05.

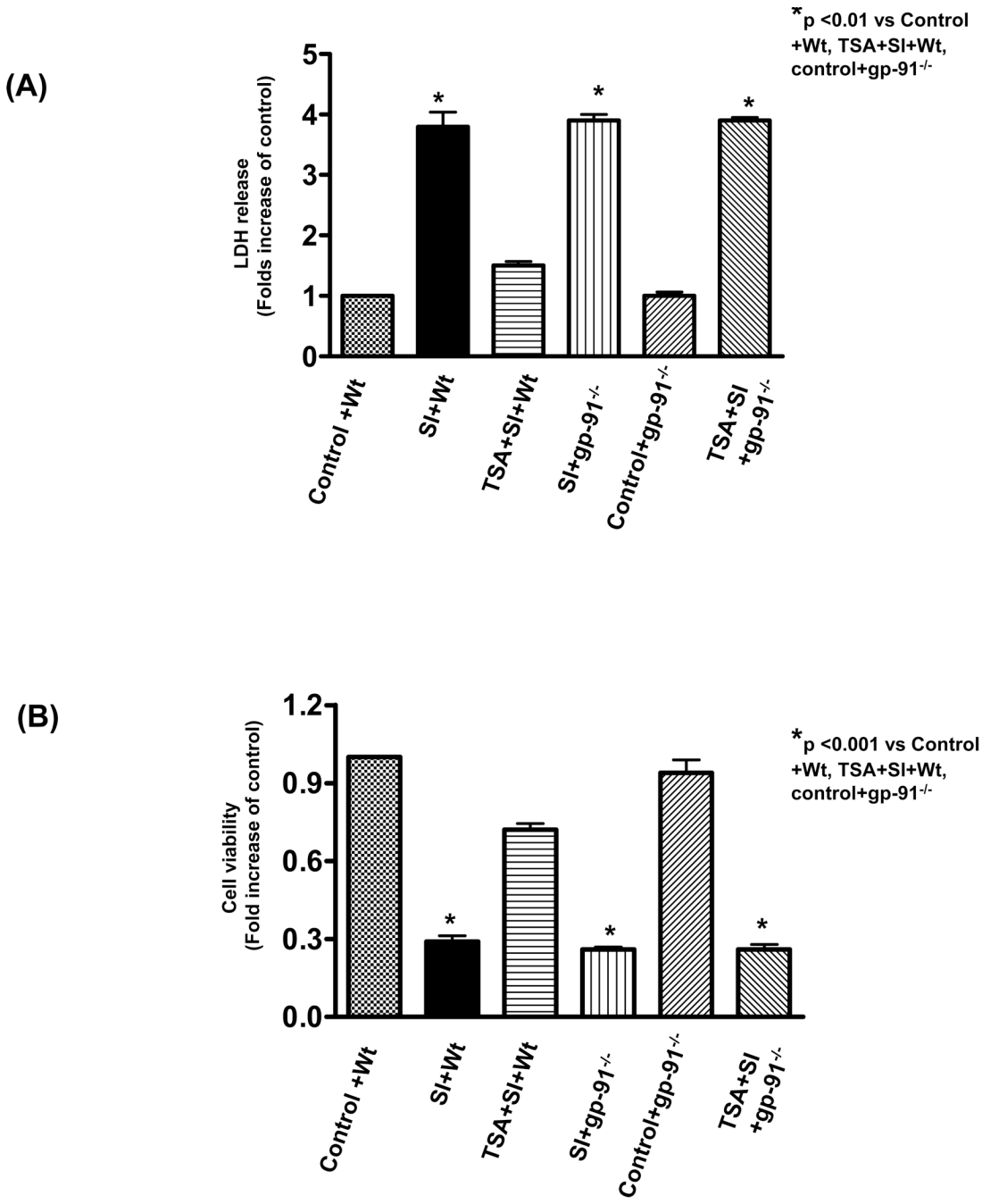

Figure 7.

(A): The LDH release in culture medium at the end of reperfusion in PLB-985 wild type and gp91^{phox}-deficient PLB-985 cells; (B): Cell viability was measured using the MTT cell viability assay. PLB-985 wild-type and gp91^{phox}-deficient PLB-985 cells were exposed to simulated ischemia (KCN and 2-deoxy-D-glucose) and description of simulated ischemia is provided under METHODS. HDAC inhibitor, trichostatin A (50 nmol/L) was maintained in culture medium. LDH: lactate dehydrogenase. Results are expressed as means ± SE and the values expressed as percentages of control values (n=4/group). SI: Simulated ischemia; Wt: wild-type PLB-895 cells; Control: Without simulated ischemia. *P < 0.01.

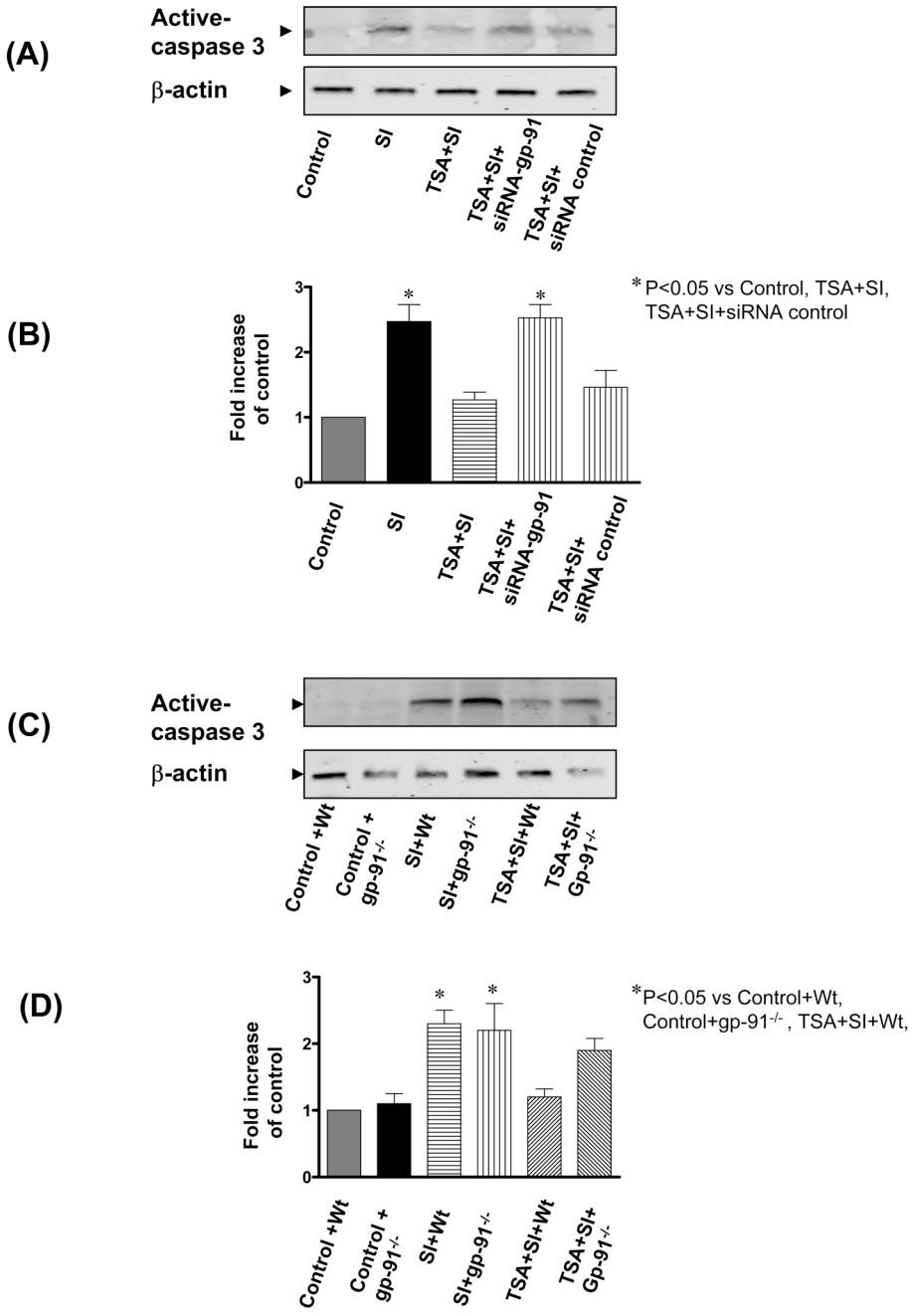

Figure 8.

(A): Representative Western blots of caspase-3 in H9c2 cardiomyoblast cells exposed to simulated ischemia; blots were probed with anti-active caspase-3; (B): The densitometric signal was normalized to the control group and expressed as a percentage. (C): Representative immunoblot showing active caspase-3 in PLB-985 wild type and gp91^{phox}-deficient PLB-985 cells. (D): The densitometric signal was normalized to the control group and expressed as a percentage. SI: Simulated ischemia; Wt: wild-type PLB-985 cells; Control: Without simulated ischemia. Results are expressed as means ± SE and the values expressed as percentages of control values (n=3/group). *P < 0.05.